

# Naval Research Laboratory

Washington, DC 20375-5000



NRL Memorandum Report 6808

AD-A237 269



## Beam Trapping in the NRL Modified Betatron Accelerator

C. A. KAPETANAKOS, D. DIALETIS,<sup>a</sup> S. J. MARSH,<sup>b</sup>  
L. K. LEN<sup>c</sup> AND T. SMITH<sup>c</sup>

*Beam Physics Branch  
Plasma Physics Division*

<sup>a</sup>*Science Applications International, Corp.*

<sup>b</sup>*SFA, Inc.,*

<sup>c</sup>*FM Technologies, Inc.*

May 15, 1991

DTIC  
ELECTED  
JUN 25 1991  
S B D

Supported by ONR and SPAWAR

91-02948



Approved for public release; distribution unlimited.

# REPORT DOCUMENTATION PAGE

Form Approved  
OMB No 0704-0188

Public reporting burden for this collection of information is estimated to average 1 hour per response, including the time for reviewing instructions, searching existing data sources, gathering and maintaining the data needed, and completing and reviewing the collection of information. Send comments regarding this burden estimate or any other aspect of this collection of information, including suggestions for reducing the burden, to Washington Headquarters Services, Directorate for Information Operations and Reports, 1215 Jefferson Davis Highway, Suite 1204, Arlington, VA 22202-4302, and to the Office of Management and Budget, Paperwork Reduction Project (0704-0188), Washington, DC 20503.

<p>1. AGENCY USE ONLY (Leave blank)</p>	<p>2. REPORT DATE 1991 May 15</p>	<p>3. REPORT TYPE AND DATES COVERED Interim</p>	
<p>4. TITLE AND SUBTITLE  Beam Trapping in the NRL Modified Betatron Accelerator</p>		<p>5. FUNDING NUMBERS  TA - RR011-09-41 WU - 1485 TA - XV-11133 WU - 2835</p>	
<p>6. AUTHOR(S)  C. A. Kapetanakos, D. Dialetis,<sup>a</sup> S. J. Marsh,<sup>b</sup> K. L. K. Len<sup>c</sup> and T. Smith<sup>c</sup></p>		<p>7. PERFORMING ORGANIZATION NAME(S) AND ADDRESS(ES)  Naval Research Laboratory Plasma Physics Division Code 4795 Washington, DC 20695-5000</p>	
<p>8. PERFORMING ORGANIZATION REPORT NUMBER  NRL Memorandum Report 6808</p>		<p>9. SPONSORING/MONITORING AGENCY NAME(S) AND ADDRESS(ES)  Office of Naval Research Arlington, VA 22217-5000</p>	
<p>10. SPONSORING/MONITORING AGENCY REPORT NUMBER</p>		<p>11. SUPPLEMENTARY NOTES  *Supported by ONR and SPAWAR, <sup>a</sup>Science Applications International, Corp., <sup>b</sup>SFA, Inc., <sup>c</sup>FM Technologies, Inc.</p>	
<p>12a. DISTRIBUTION/AVAILABILITY STATEMENT  Approved for public release; distribution unlimited.</p>		<p>12b. DISTRIBUTION CODE</p>	
<p>13. ABSTRACT (Maximum 200 words)  The experimental results on the trapping of the beam in the NRL modified betatron accelerator are in good agreement with a revised model of resistive trapping and thus it may be concluded that the wall resistivity is responsible for the inward spiral motion of the beam after injection.</p>			
<p>14. SUBJECT TERMS  Accelerator High energy beams</p>		<p>15. NUMBER OF PAGES 21</p>	
<p>16. PRICE CODE</p>			
<p>17. SECURITY CLASSIFICATION OF REPORT Unclassified</p>	<p>18. SECURITY CLASSIFICATION OF THIS PAGE Unclassified</p>	<p>19. SECURITY CLASSIFICATION OF ABSTRACT Unclassified</p>	<p>20. LIMITATION OF ABSTRACT SAR</p>

## CONTENTS

INTRODUCTION.....	1
BRIEF DESCRIPTION OF THE EXPERIMENT .....	2
EXPERIMENTAL RESULTS .....	2
COMPARISON WITH THEORY.....	5
TABLE .....	10
REFERENCES .....	12



Accession For	
NTIS GRA&I	<input checked="" type="checkbox"/>
DTIC TAB	<input type="checkbox"/>
Unannounced	<input type="checkbox"/>
Justification	
By _____	
Distribution/	
Availability Codes	
Dist	Avail and/or Special
A-1	

## BEAM TRAPPING IN THE NRL MODIFIED BETATRON ACCELERATOR

**Introduction.** – Currently, several laboratories<sup>1-5</sup> are engaged in studies to assess the feasibility of compact, high current accelerators. Among the various accelerating schemes presently under investigation is the Modified Betatron Accelerator (MBA). This device is under study at the University of California, Irvine<sup>2</sup> and also at the Naval Research Laboratory (NRL). Since the initial successful demonstration of acceleration<sup>1</sup> approximately two years ago, the NRL-MBA has achieved<sup>9</sup> trapped currents as high as 1.5 kA and energies approximately 18 MeV. The beam lifetime that is typically 700-900  $\mu$ sec is limited by the cyclotron resonance.

Following the installation of strong focusing windings<sup>9, 10</sup> in the NRL device it is routinely observed<sup>1, 11</sup> that for several combinations of injection parameters the beam consistently spirals from the injection position to the magnetic minor axis and is trapped. The explanation of this interesting phenomenon has been so far elusive. However, a fair understanding of the trapping mechanism is not only of academic interest but a necessity for any upgrading of the existing or the construction of a new device.

In this paper we report recent experimental results on the trapping of the beam in the NRL-MBA. The results are in agreement with a revised model of resistive trapping<sup>12</sup>. Two modifications have been introduced to the original model. First, the beam motion is not limited near the minor axis and therefore nonlinear effects and the fast diffusion times that scale as  $\mu_0(b - a)^2/\pi^2\rho$ , where  $(b - a)$  is the thickness of the chamber and  $\rho$  is the wall resistivity, become important. Second, in order to take into account the intermediate motion<sup>10</sup> of the beam that has been omitted in the calculation of the image fields of the beam, the wall surface resistivity is computed using the skin depth that corresponds to the frequency of the intermediate mode and not the actual thickness of the chamber.

There are three distinct groups of diffusion times with which the self magnetic field of the beam leaks out of a resistive torus. The shortest are the “plane” characteristic times  $\tau_{mk} \approx \mu_0(b - a)^2/\pi^2\rho k^2 = \frac{\tau_{01}}{k^2} \equiv \frac{\tau_p}{k^2}$  where  $k = 1, 2, 3, \dots$ . The “plane” diffusion

---

Manuscript approved April 3, 1991.

times are important when the beam is near the wall. The "cylinder" diffusion times are  $\tau_{m0} \approx \tau_{10}/m = \tau_c/m = \mu_0 a(b-a)/2\rho m$ , where  $m = 1, 2, 3, \dots$ . Both  $\tau_p$  and  $\tau_c$  determine the speed with which the self magnetic field of the beam penetrates the wall of the chamber and are instrumental in the resistive trapping of the beam. Finally, the "loop" diffusion time  $\tau_{00} \equiv \tau_\ell = 2\tau_c [\ln \frac{8r_0}{a} - 2]$ , where  $r_0$  is the major radius of the torus, determines the speed with which the beam field diffuses into the hole of the doughnut. The "loop" diffusion time does not play any role in the resistive trapping of the beam.

The resistive trapping is due to the negative radial component of the image magnetic field of the beam that acts on its centroid, when such a beam moves poloidally inside a resistive chamber. This field component crossed with the axial (toroidal) velocity of the beam produces a poloidal force, which is in the opposite direction to the poloidal motion of the beam. In the absence of the strong focusing and when the self-fields dominate the external fields (high current regime), the poloidal force in conjunction with the axial (toroidal) magnetic field drives the beam to the wall (drag instability<sup>13</sup>). However, in the presence of strong focusing the direction of the poloidal motion can be reversed and the beam spirals to the minor axis.<sup>12</sup>

**Brief Description of the Experiment.** – The NRL modified betatron has been described<sup>1, 14</sup> previously. In this paper we give, for completeness, a short description of its basic components. The NRL-MBA is a toroidal device that comprises three different external magnetic fields; the betatron field  $B_z$  that can vary from 0-2.7 kG, the toroidal field  $B_\theta$  that can vary between 0-5.1 kG and the strong focusing field that has a maximum gradient between 0-31 G/cm, when the current  $I_{SF}$  in the windings varies from 0-30 kA.

The 100-cm major radius, 15.2-cm-inside minor radius vacuum chamber has been constructed using epoxy-reinforced carbon fibers. The desired conductivity is obtained by embedding in the outer layer of graphite a phosphor bronze screen. The measured dc resistance of the toroidal vessel is  $68 \pm 2 m\Omega$  and the corresponding surface resistivity is  $10.3 m\Omega$  on a square. The graphite surface resistivity is  $26.6 m\Omega$  on a square.

The electrons are emitted from one-end-face of a cylindrical carbon cathode. The other end-face is mounded on the cathode stalk. The emitting surface of the cathode faces the circular opening of the conical anode, that is located on the midplane of the device 8.7 cm from its minor axis.

**Experimental Results.** – Over a wide range of parameters and after fine tuning the external fields the beam spirals from the injector near the minor axis and is trapped. The

beam trapping time, i.e., the time it takes the beam to travel from the injection position to the vicinity of the minor axis is determined by measuring the time delay between the x-ray peaks that are generated at injection and at a  $1 \times 1.1\text{-cm}$ , 0.8-mm thick lead target that is located on the magnetic minor axis. The lead target is mounted on the front surface of a  $3\text{-}\mu\text{m}$ -thick polycarbonate foil that is stretched across the minor cross section of the vacuum chamber as shown in Fig. 1a. The x-rays are monitored by a collimated x-ray detector that is located 4-m away from the lead target. The scintillator-photomultiplier tube is housed inside a lead box and the x-rays enter the scintillator through a 3-mm-dia. hole. The foil is graphite coated on the upstream side to avoid charging. Figure 1b shows an open-shutter photograph of the light emitted as the beam passes through the foil. The x-rays emitted as the beam strikes the diode and the lead target are shown in the upper trace of Fig. 1c. The trapping time  $\tau_{tr}$  for this shot is  $1.25\text{ }\mu\text{sec}$ . The lower trace of Fig. 1c shows the output of the Rogowski coil that monitors the beam current. The peak of the signal corresponds to  $1.2\text{ kA}$ .

The results shown in Fig. 1 were taken with a 0.5-cm hole in the anode. This hole is by a factor of three smaller than that used regularly in the NRL device. Thus, the trapped current has been reduced by a factor of 2-3. This reduction in the beam current was necessary in order to achieve satisfactory resolution in the open-shutter photographs.

To determine the effect of the foil on the transverse beam orbit, we carried out a series of experiments in which the  $3\text{-}\mu\text{m}$  thick foil was replaced with a foil of the same composition but with only half its thickness. The results show that the equilibrium position of the beam is slightly larger in the case of  $1.5\text{ }\mu\text{m}$  thick foil. It requires approximately 1-2 G higher vertical field ( $\sim 4 - 8\%$ ) to shift the equilibrium to its original position and make the orbits identical.

As the electrons pass through the plastic foil, they suffer both inelastic and elastic scattering. The stopping power<sup>15</sup> of 0.6 MeV electrons passing through polyethylene (data for polycarbonate are not available) is  $\sim 2\text{ (MeV-cm}^2\text{)}/\text{gm}$ . Thus, the energy loss per pass is 0.6 keV. The total energy loss in  $1.2\text{ }\mu\text{sec}$ , i.e., in sixty revolutions around the major axis is 36 keV or  $\sim 6\%$ . The energy loss in the thinner foil is only 18 keV and therefore, the equilibrium position is expected to increase by 3% when the thickness of the foil is reduced to half. This shift is not substantially different to that observed in the experiment. The elastic scattering induced RMS angle is  $0.9^\circ$  for the first pass through the  $1.5\text{ }\mu\text{m}$  thick foil. Although substantial, the elastic scattering does not contribute to the shift of the equilibrium position.

The beam orbits are very reproducible and  $\tau_{tr}$  shows only modest variations for the same operating parameters. Figure 2a shows  $\tau_{tr}$  for seven shots taken with the same values of the fields. It is apparent from this figure that  $\tau_{tr}$  varies by  $\pm 7\%$ . In a second run with five shots the variation was even smaller. Figure 2b shows  $\tau_{tr}$  vs.  $B_\theta$  for constant  $I_{SF}/B_\theta$ . For all practical purposes  $\tau_{tr}$  remains constant in the narrow range tested.

In addition to  $\tau_{tr}$ , the bounce period  $\tau_B$ , i.e., the time the beam takes to perform a complete revolution in the poloidal direction, is of special interest. To determine  $\tau_B$ , the foil target was removed and replaced with a 1.1-cm wide, 1-mm thick, 16-cm long lead strip. The lead target is backed on the upstream side, by a thin plastic strip and is mounted of a half lucite ring that is carbon coated. The symmetry axis of the target lies on the midplane of the device as shown in Fig. 3a.

The light emitted from the upstream side of the target when the beam strikes it, is monitored with an open shutter camera. Results are shown in Fig. 3b. The x-ray signal and the output of the Rogowski coil that monitors the beam current are shown in Fig. 3c. The bounce period is inferred from the time delay of the two x-ray peaks, as indicated in Fig. 3c, and in this shot is 840 nsec. The damage pattern on the lead strip has a diameter that is equal to the diameter of the anode hole. This implies that the diameter of the beam has not changed after about 40 revolutions around the major axis. In addition, we observe that the damage pattern is a semi-circle that is located always near the lower edge of the strip. From this observation it may be concluded that the beam drifts 3mm over 20 nsec, i.e., its bounce speed near the strip is  $\sim 15 \text{ cm}/\mu\text{sec}$ .

To verify that there is not correlation between  $\tau_{tr}$  and  $\tau_\ell$ , i.e., with the speed the beam magnetic field diffuses into the hole of the doughnut, the vacuum chamber was unbolted in two joints that are located  $180^\circ$  apart in the toroidal direction and a ring insulator was inserted in each of these joints. Sixty carbon resistors,  $51\Omega$  each were symmetrically mounted on the outer surface of one of the two rings as shown in Fig. 4a. To improve its voltage holding capabilities the inner surface of the blue nylon insulator was angled and a 0.6 cm deep groove was machined at its plane of symmetry. In addition, its inner surface was protected from stray electrons by a 0.8 mm thick lead strap that is supported by an epoxy reinforced carbon fiber belt. The purpose of the second insulator was only to minimize the distortion of the toroidal chamber and thus shorting wide straps, instead of resistors, were installed on its outer surface.

There are two distinct currents flowing on the wall of the vacuum chamber. The first  $i_w$  is due to the rising vertical field and the second  $I_r$  is induced by the beam. Since the vertical

field during the first quarter period varies as  $B_z(t) = B_{zp} \sin(2\pi t/\tau)$ , where  $B_{zp}$  is the peak field and  $\tau$  is the period, the induced voltage in the chamber is  $V = -V_0 \cos(2\pi t/\tau)$ , where  $V_0 = (4\pi^2 r_0^2/\tau) B_{zp}$  and  $r_0$  is the major radius of the torus. The current flowing on the wall of the chamber is described by the equation  $V = L \frac{di_w}{dt} + Ri_w$ , where  $L$  is the inductance and  $R$  the resistance of the torus. The instantaneous value of  $i_w$  can be found by integrating the above equation and is given by

$$i_w = -\frac{V_0}{R \left[ 1 + \left( \frac{2\pi L/R}{\tau} \right)^2 \right]} \left[ \cos(2\pi t/\tau) + \frac{2\pi L/R}{\tau} \sin(2\pi t/\tau) - e^{-t/(L/R)} \right], \quad (1)$$

with the initial condition  $i_w(t = 0) = 0$ .

The temporal profile of  $i_w$  predicted by the above simple model is identical to that predicted from the exact solution of the diffusion problem for a toroidal resistive shell<sup>16</sup> and also is in good agreement with the results of TRIDIF code for a finite thickness toroidal vessel. According to Eq.(1),  $i_w$  has a maximum at time  $t_p$ , which for  $\alpha \equiv 2\pi(L/R)/\tau \ll 1$  is determined from  $\alpha^2 [1 - t_p/(L/R)] = -e^{-t_p/(L/R)}$ . The peak value of the current is  $i_{wp} = V/R$ . The measured peak value of the current in the experiment is in good agreement with the above theoretical prediction and scales, as expected, with the value of the resistance at the gap.

The return current of the beam is measured with a fast Rogowski coil ( $\tau_{\text{rise}} \approx 20\text{nsec}$ ) that is located in the outside of the vacuum chamber. With the resistors at the gap shorted, the Rogowski coil shows a slowly rising current that is consistent with the decay of  $I_r$ . However, when the shorting clips are removed the Rogowski coil shows a current pulse that rises to  $\sim 2/3$  of its peak value in less than 100 nsec as shown in Fig. 4b. The lower trace in Fig. 4b shows the voltage across the resistors  $V_g$  as measured directly by a Tektronix 7844 oscilloscope after a 100 X attenuation. The shape of the time integrated  $V_g$  is very similar to the current waveform registered by the Rogowski coil, i.e.,  $V_g$  is proportional to the time derivative of the current.

**Comparison with Theory** – The equations that describe the motion of the beam centroid have been solved numerically using analytical expressions for  $B_z$  and  $B_\theta$ . The stellarator fields are determined numerically from Biot-Savart law by dividing each period of the windings into twenty segments. The image fields on the beam centroid have been computed analytically for a uniform density electron ring that is located inside a large major radius torus with resistive wall of thickness  $b-a$ , where  $a$  is the inner and  $b$  the outer

radii of the torus. In contrast with previous calculation<sup>12</sup>, the beam is not limited near the minor axis.

In the local cylindrical coordinate system  $(\rho, \phi, z)$  with its origin on the geometric minor axis, the electrostatic potential inside the ring is given by<sup>17</sup>

$$\begin{aligned}\Phi_0 = & \frac{Q_\ell}{2\pi\epsilon_0} \left[ \ell n \frac{a}{r_b} + \frac{1}{2} - \frac{1}{2} \frac{\rho^2 + \Delta^2 - 2\Delta\rho \cos(\phi - \alpha)}{2r_b^2} \right. \\ & \left. + \frac{1}{2} \ell n \left( 1 + \left( \frac{\Delta\rho}{a^2} \right)^2 - 2 \frac{\Delta\rho}{a^2} \cos(\phi - \alpha) \right) \right],\end{aligned}\quad (2)$$

where  $\Delta$  and  $\alpha$  define the beam position on the transverse plane,  $r_b$  is the minor radius of the beam and  $Q_\ell$  is the charge per unit length. Similarly, the magnetic vector potential inside the beam is<sup>17</sup>

$$\begin{aligned}A_{\theta 0} = & \frac{\Phi_0 \beta_\theta}{c} + \sum_{k=0}^{\infty} A_{ok} U_{ok}^{(c)}(t) \\ & + \sum_{m=1}^{\infty} \sum_{k=0}^{\infty} A_{mk} \left( \frac{\rho}{a} \right)^m \left[ U_{mk}^{(c)}(t) \cos m\phi + U_{mk}^{(s)}(t) \sin m\phi \right],\end{aligned}\quad (3)$$

where  $\beta_\theta$  is the normalized toroidal beam velocity.

The time dependent coefficients  $U_{mk}^{(c)}(t)$ ,  $U_{mk}^{(s)}(t)$  are zero at  $t = 0$  and are determined by the differential equations

$$\dot{U}_{mk}^{(c)} + \frac{1}{\tau_{mk}} U_{mk}^{(c)} = \frac{Q_\ell \beta_\theta}{2\pi\epsilon_0 c \tau_{mk}} \left( \frac{\Delta}{\alpha} \right)^m \cos m\alpha, \quad (4)$$

$$\dot{U}_{mk}^{(s)} + \frac{1}{\tau_{mk}} U_{mk}^{(s)} = \frac{Q_\ell \beta_\theta}{2\pi\epsilon_0 c \tau_{mk}} \left( \frac{\Delta}{\alpha} \right)^m \sin m\alpha, \text{ where } \frac{1}{\tau_{mk}} = \frac{\alpha_{mk}^2}{\mu_0 \sigma},$$

$$m = 0, 1, 2, \dots, \quad k = 0, 1, 2, \dots,$$

$\sigma$  is the wall conductivity of the toroidal chamber and  $\alpha_{mk}$  are the zeros of the function

$$\begin{aligned}f_0(\alpha) = & \frac{\pi}{2} x_0 [J_1(x_0)Y_0(x_1) - Y_1(x_0)J_0(x_1)] \\ & - \frac{\pi}{2} \left( \ell n \frac{8R_b}{b} - 2 \right) x_0 x_1 [J_1(x_0)Y_1(x_1) - Y_1(x_0)J_1(x_1)],\end{aligned}\quad (5)$$

when  $m = 0$ , and

$$f_m(\alpha) = \frac{\pi}{4} x_0 x_1 [J_{m+1}(x_0)Y_{m-1}(x_1) - Y_{m+1}(x_0)J_{m-1}(x_1)], \quad (6)$$

when  $m=1,2,3,\dots$ . The arguments of Bessel functions in (5) and (6) are  $x_0 = \alpha a$ ,  $x_1 = \alpha b$  and  $R_b$  is the major radius of the beam. For each  $m$  there is an infinite number of zeros denoted by the index  $k = 0,1,2,\dots$ . The time independent coefficients  $A_{0k}$ ,  $A_{mk}$ , that appear in the vector potential are equal to

$$A_{mk} = -\frac{2g_m(\alpha_{mk})}{\alpha_{mk}f'_m(\alpha_{mk})},$$

where  $f'_m(\alpha)$  is the derivative of  $f_m(\alpha)$  and

$$g_0(\alpha) = \frac{\pi}{2} [J_0(x_0)Y_0(x_1) - Y_0(x_0)J_0(x_1)] - \frac{\pi}{2} \left( \ln \frac{8R_b}{b} - 2 \right) x_1 [J_0(x_0)Y_1(x_1) - Y_0(x_0)J_1(x_1)],$$

when  $m=0$ , and

$$g_m(\alpha) = \frac{\pi}{2} x_1 [J_m(x_0)Y_{m-1}(x_1) - Y_m(x_0)J_{m-1}(x_1)],$$

when  $m=1,2,3,\dots$ . The image fields at the beam centroid, i.e., when  $\rho = \Delta$  and  $\phi = \alpha$ , are obtained from the expressions of  $\Phi_0$  and  $A_{\theta 0}$  given above.

The radial components  $B_\rho^{(c)}$  at the beam centroid is of special interest because it is responsible for the inward radial motion of the beam. This component is given by

$$B_\rho^{(c)} = \sum_{m=1}^{\infty} \sum_{k=0}^{\infty} \frac{m}{a} A_{m,k} \left( \frac{\Delta(t)}{a} \right)^{m-1} * \left[ -U_{mk}^{(s)}(t) \cos m\alpha(t) + U_{mk}^{(c)}(t) \sin m\alpha(t) \right]. \quad (7)$$

Since  $B_\rho^{(c)}$  is independent of  $A_{0k}$  and  $U_{0k}^{(c)}$ , i.e., it is independent of loop time  $\tau_\ell = \tau_{00}$ , the beam trapping time should also be independent of  $\tau_\ell$  as observed in the experiment.

To gain further insight, we have computed the image fields, including first order toroidal corrections, at the beam centroid for a beam inside a resistive toroidal shell. In this case,  $B_\rho^{(c)}$ .

$$B_\rho^{self} = \frac{\sin \alpha}{R_b} \left[ \frac{Q_\ell \beta_\theta}{4\pi \epsilon_0 c} \left( \ln \frac{a}{r_b} + 1 \right) + \frac{Q_\ell \beta_\theta}{4\pi \epsilon_0 c} \ln \left( 1 - \left( \frac{\Delta(t)}{a} \right)^2 \right) - \frac{Q_\ell \beta_\theta}{16\pi \epsilon_0 c} \left( \frac{r_b}{a} \right)^2 \frac{1}{\left[ 1 - \left( \frac{\Delta}{a} \right)^2 \right]^2} \right. \\ \left. + \frac{1}{2} \sum_{m=1}^{\infty} \frac{1}{m} \left( \frac{\Delta(t)}{a} \right)^m \left( U_{cm}^{(0)}(t) \cos m\alpha(t) + U_{sm}^{(0)}(t) \sin m\alpha(t) \right) \right]$$

$$\begin{aligned}
& + \frac{1}{2} \left( \ell n \frac{8R_b}{a} - 2 \right) U_0^{(0)}(t) + U_0^{(1)}(t) \Big] \\
& + \frac{1}{a} \sum_{m=1}^{\infty} \left( \frac{\Delta(t)}{a} \right)^{m-1} \left[ - \left( U_{sm}^{(0)}(t) + U_{sm}^{(1)}(t) + V_{sm}^{(1)}(t) \right) \cos m\alpha \right. \\
& \quad \left. + \left( U_{cm}^{(0)}(t) + U_{cm}^{(1)}(t) + V_{cm}^{(1)}(t) \right) \sin m\alpha(t) \right], \quad (8)
\end{aligned}$$

where the time-dependent parameters  $U_0^{(0)}(t)$ ,  $U_0^{(1)}(t)$ ,  $U_{cm}^{(0)}(t)$ ,  $U_{sm}^{(0)}(t)$ ,  $U_{cm}^{(1)}(t)$ ,  $U_{sm}^{(1)}(t)$ ,  $V_{cm}^{(1)}(t)$  and  $V_{sm}^{(1)}(t)$  are zero at  $t = 0$  and are determined by the differential equations.

$$\begin{aligned}
\dot{U}_0^{(0)} + \frac{1}{\tau_\ell} \left( 1 + \tau_c \frac{\dot{x}_c}{R_b} \right) U_0^{(0)} &= \frac{2Q_\ell \beta_\theta}{4\pi\epsilon_0 c} \frac{1}{\tau_\ell} \left( 1 + \frac{x_c}{2R_b} \right), \\
\dot{U}_0^{(1)} + \frac{1}{\tau_c} U_0^{(1)} &= \frac{1}{2\tau_c} U_0^{(0)}, \\
\dot{U}_{cm}^{(0)} + \frac{m}{\tau_c} U_{cm}^{(0)} &= \frac{2Q_\ell \beta_\theta}{4\pi\epsilon_0 c} \frac{m}{\tau_c} \left( \frac{\Delta}{a} \right)^m \cos m\alpha, \\
\dot{U}_{sm}^{(0)} + \frac{m}{\tau_c} U_{sm}^{(0)} &= \frac{2Q_\ell \beta_\theta}{4\pi\epsilon_0 c} \frac{m}{\tau_c} \left( \frac{\Delta}{a} \right)^m \sin m\alpha, \\
\dot{U}_{cm}^{(1)} + \frac{m}{\tau_c} U_{cm}^{(1)} &= - \frac{\dot{x}_c}{2R_b} U_{cm}^{(0)}, \quad (9) \\
\dot{U}_{sm}^{(1)} + \frac{m}{\tau_c} U_{sm}^{(1)} &= - \frac{\dot{x}_c}{2R_b} U_{sm}^{(0)}, \\
\dot{V}_{cm}^{(1)} + \frac{m}{\tau_c} V_{cm}^{(1)} &= \frac{Q_\ell \beta_\theta}{16\pi\epsilon_0 c} \frac{m^2}{\tau_c} \frac{a}{R_b} \left( \frac{r_b}{a} \right)^2 \left( \frac{\Delta}{a} \right)^{m-1} \cos(m-1), \\
\dot{V}_{sm}^{(1)} + \frac{m}{\tau_c} V_{sm}^{(1)} &= \frac{Q_\ell \beta_\theta}{16\pi\epsilon_0 c} \frac{m^2}{\tau_c} \frac{a}{R_b} \left( \frac{r_b}{a} \right)^2 \left( \frac{\Delta}{a} \right)^{m-1} \sin(m-1)\alpha,
\end{aligned}$$

where

$$\tau_0 = 2\tau_c \left[ \ell n \frac{8R_b}{a} - 2 - \frac{x_c}{2R_b} \right],$$

and

$$x_c = \Delta \cos \alpha \equiv R_b - r_0.$$

It is apparent from Eqs. (8) and (9) that the toroidal correction term of  $B_\rho^{(c)}$  is a function of  $\tau_\ell$ . However, this term is multiplied by  $\sin \alpha(t)$  and therefore averages to zero in a poloidal period.

In the limit  $(b - a) \ll a$ , the toroidal electric field  $E_\theta$  on the outer surface of the chamber for a stationary beam has a relatively simple, closed form. At  $t = 0$ ,  $E_\theta = 0$  and

peaks within a few fast diffusion times  $\tau_p$ . For a longer time,  $E_\theta$  decays to zero with  $\tau_\ell$ . This form of the electric field is consistent with the observed return current after the beam injection. When the resistors at the gap are shorted the current measured with the external Rogowski coil should rise at the same rate the beam return current decays. However, when the resistors at the gap are not shorted, a portion ( $I_{r1}$ ) of the return current ( $I_r$ ) flows on the outer wall of the chamber as shown in Fig. 4.  $I_{r1}$  rises considerably faster because the beam magnetic field can leak locally out of the resistive gap considerably faster than it can leak out of a uniform chamber.

Results from the numerical integration of orbit equations are shown in Fig. 5. The various parameters for the run are listed in Table I. Figure 5a shows the projection of the centroid's orbit on the  $\theta = 0$  plane. Both the intermediate and slow (bounce) modes are apparent. Since there are six field periods between  $0 \leq \theta \leq 2\pi$ , the electrons perform six oscillations during one revolution around the major axis. To take into account the intermediate motion that has been neglected in the calculation of the image fields, the surface resistivity in the code is computed using the skin depth that corresponds to the intermediate frequency and not the actual thickness of the wall.

The solid circles in Fig. 5b show the positions the beam crosses the  $\theta = 240^\circ$  plane. This is a realistic simulation of the experimental situation. The time difference between two circles is equal to the period around the major axis, i.e.,  $\sim 23$  nsec. The parameters of this run are similar to those in Fig. 5c and the similarity of the two orbits is quite apparent.

There is some ambiguity, both in the experiment and theory, in the determination of the beam trapping time, because its exact value depends on the position and size of the target. However, this is not the case with  $\tau_B$ , which can be measured very accurately. We make four runs for different values of  $B_\theta$  keeping  $I_{SF}/B_\theta = \text{constant}$ . Figure 2b shows  $\tau_B$  vs.  $B_\theta$  for three of these runs. For all practical purposes  $\tau_B$  remains constant as  $B_\theta$  varies. In the fourth run  $B_\theta$  was reduced to 2 kG and although the beam orbit changed substantially  $\tau_B$  was lower only by 7%.

As a rule, the theory predicts a  $\tau_B$  and  $\tau_{tr}$  that are approximately a factor of two shorter than those observed in the experiment. With the exception of these two times the revised model of resistive trapping is in agreement with the experiment observations, although in the analysis the beam current remains constant while in the experiment the current decays. This decay is observed whenever there is a target inside the chamber but often is absent during the acceleration experiments when the various targets are removed.

**Table I.**  
**Parameters of the run shown in Fig. 5**

Torus major radius $r_0$	= 100cm
Torus minor radius $a$	= 15.2 cm
Relativistic factor $\gamma$	= 1.5
SF radius $\rho_0$	= 23.4 cm
SF current $I_{SF}$	= 24 kA
Vertical field at inj. $B_{z0}$	= 26G
Toroidal field $B_{0\theta}$	= 4 kG
Beam minor radius $r_b$	= 3 mm
Beam current $I_b$	= 1.2 kA
Wall resistivity $\rho$	= 8 $m\Omega - cm$
Intermediate freq. $\omega_W$	= $1.8 \times 10^9$ sec $^{-1}$

## Figure Captions

1. Beam trapping time.
2. Trapping time reproducibility (a) and dependance of  $\tau_{tr}$  and  $\tau_B$  on  $B_\theta$  for constant  $I_{SF}/B_\theta$ (b).
3. Beam bounce period.
4. (a) Schematic of the vacuum chamber joint with the insulator in place. (b) Current and gap voltage waveforms.
5. Beam centroid orbit from the numerical integration of the equations of motion, using the image fields from the resistive shell model (a and b). Results from the experiment (c).

## References

† This work is supported by ONR and the Space and Naval Warfare Command.

- (a) Permanent address: Science Applications International Corporation, 1710 Goodridge Drive, McLean, VA 22102.
- (b) Permanent address: SFA, Inc., Landover, MD 20785.
- (c) Permanent address: FM Technologies, Inc., 10529-B Braddock Road, Fairfax, VA 22032.

1. C.A. Kapetanakos *et al.*, Phys. Rev. Letts. **64**, 2374 (1990).
2. H. Ishizuka *et al.*, in Proceedings of the Seventh International Conference on High-Power Particle Beams, Karlsruhe, Germany, July 1988, edited by W. Bauer and W. Schmidt (Kernforschungszentrum Karlsruhe GmbH, Karlsruhe, 1988), Vol. II, P. 857.
3. S. Humphries, Jr., and L.K. Len, in Proceedings of the 1987 Particle Accelerator Conference, Washington, DC, March 1987, edited by E.R. Lindstrom and L.S. Taylor (IEEE, New York, 1987), p. 914.
4. V. Bailey *et al.*, in Proceedings of the 1987 Particle Accelerator Conference (Ref. 3), p. 920.
5. W.K. Tucker *et al.*, in Proceedings of the 1987 Particle Accelerator Conference (Ref. 3), p. 957.
6. P. Sprangle and C.A. Kapetanakos, J. Appl. Phys. **49**, 1 (1978).
7. C.A. Kapetanakos *et al.*, Phys. Fluids **26**, 1634 (1983).
8. N. Rostoker, Comments Plasma Phys. **6**, 91 (1980).
9. C. Roberson *et al.*, Phys. Rev. Letts. **50**, 507 (1983).
10. C.A. Kapetanakos *et al.*, Part. Accel. **21**, 1 (1987).
11. C.A. Kapetanakos *et al.*, Phys. Fluids (to be published), 1991.
12. P. Sprangle and C.A. Kapetanakos, Part. Accel. **18**, 203 (1986). Also Y. Seo and P. Sprangle, Part. Accel. (1991).
13. P. Sprangle and C.A. Kapetanakos, Part. Accel. **14**, 15 (1983).
14. L.K. Len *et al.*, Proc. of Int. Soc. for Opt. Eng. (SPIE) (SPIE, Bellingham, WA, 1990) Vol. 1226, p. 38.
15. M.J. Berger and S.M. Seltzer, NASA Report # SP-3012 (1964).
16. D. Dialetis *et al.*, J. Appl. Phys. **69**, 1813 (1991).
17. D. Dialetis *et al.*, Submitted to Part. Accel.

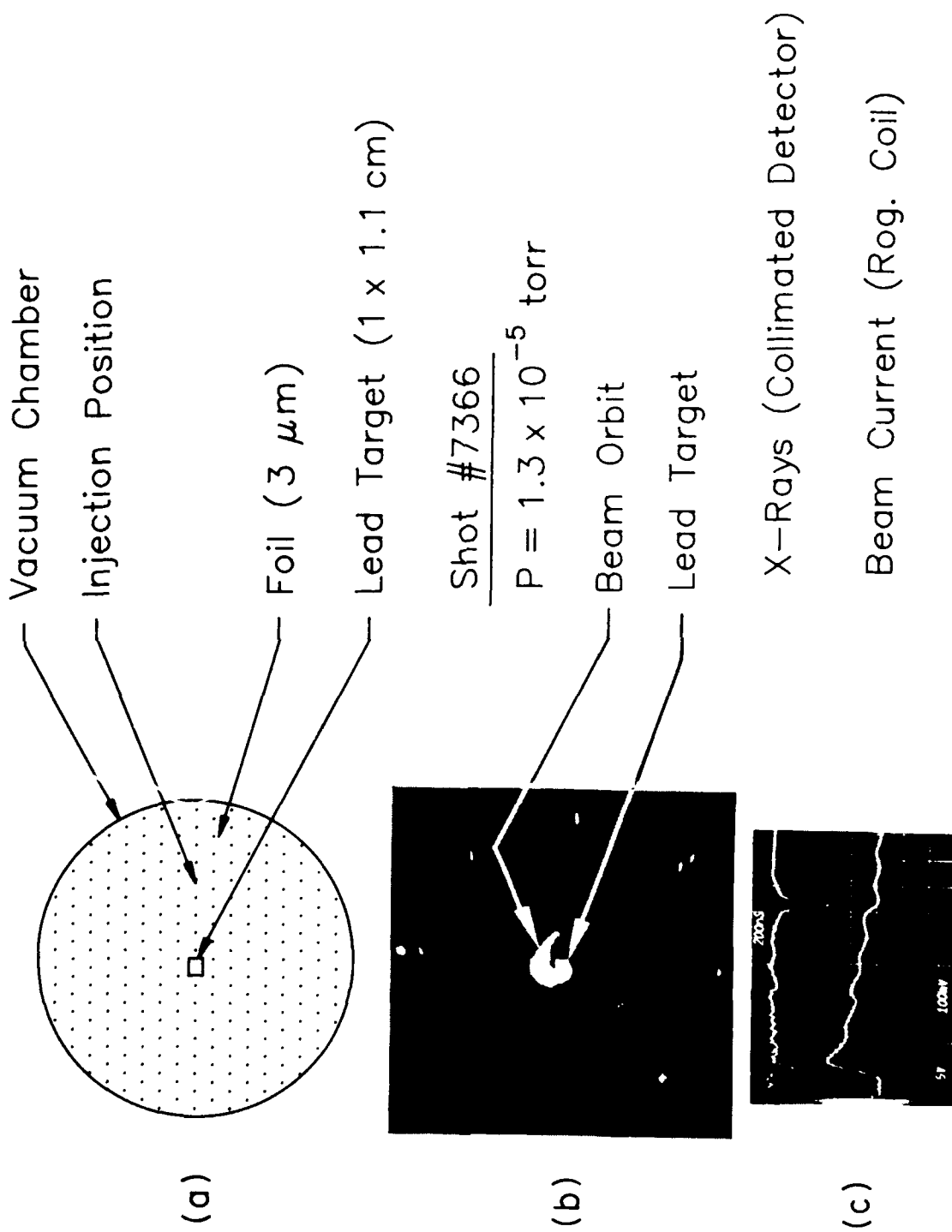


Fig. 1 - Beam trapping time

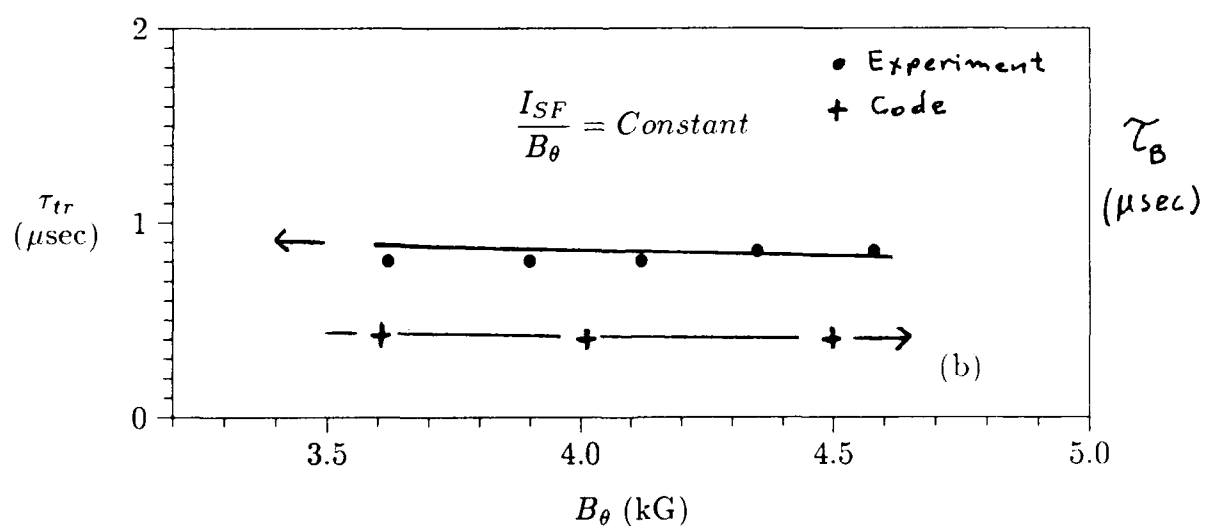
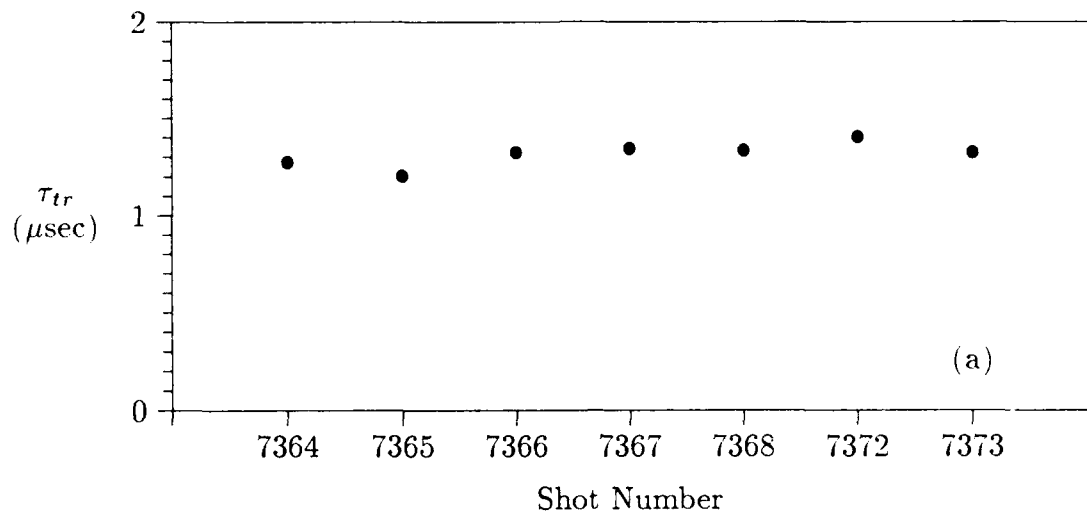


Fig. 2 — Trapping time reproducibility (a) and dependence of  $\tau_{tr}$  and  $\tau_B$  on  $B_\theta$  for constant  $I_{SF}/B_\theta$  (b).

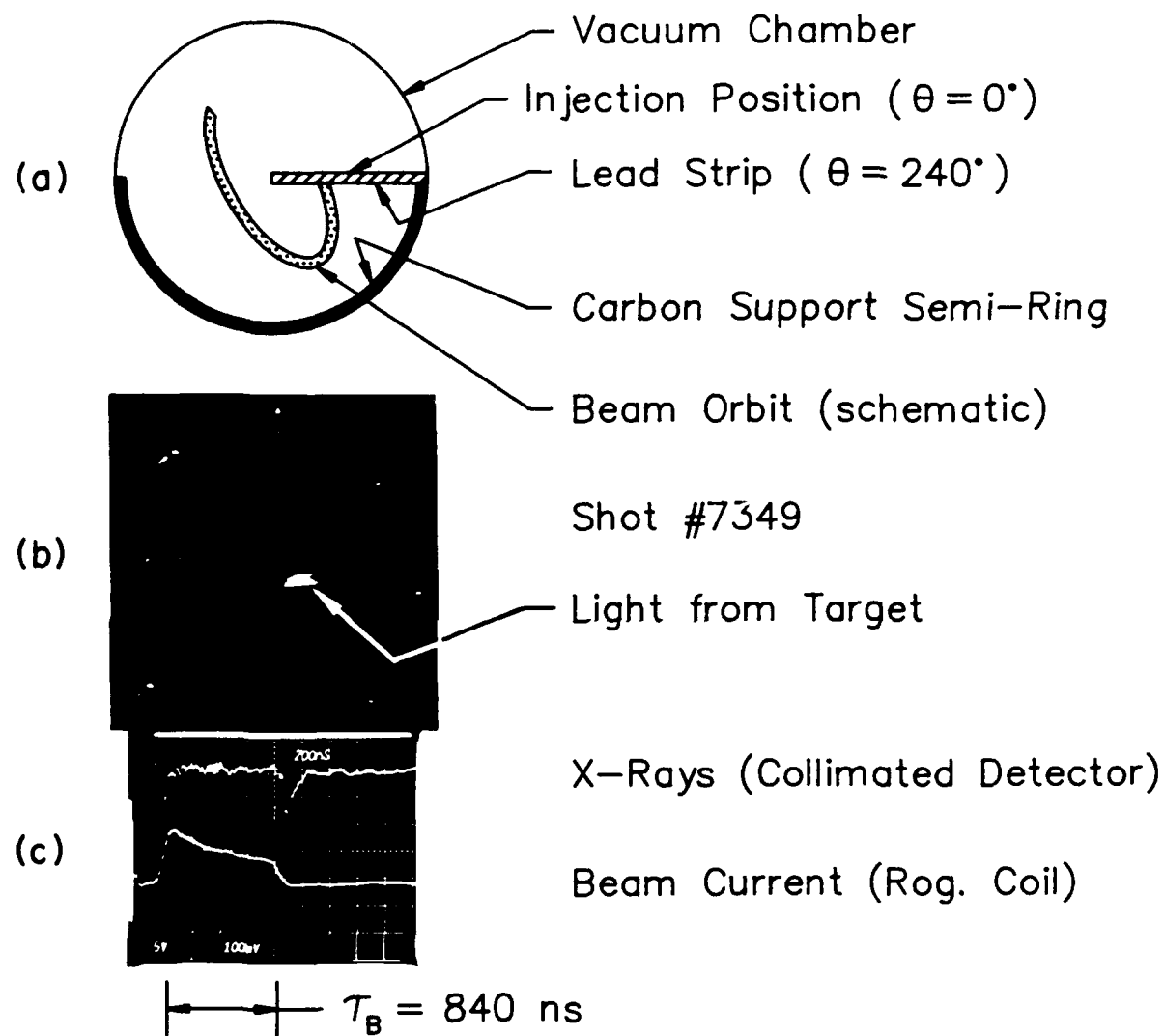


Fig. 3 — Beam bounce period

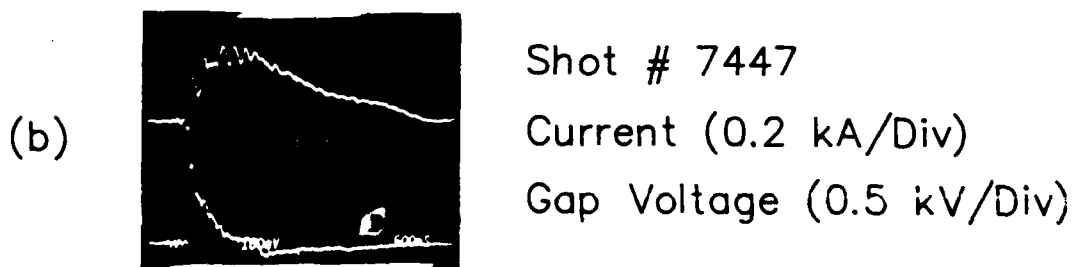
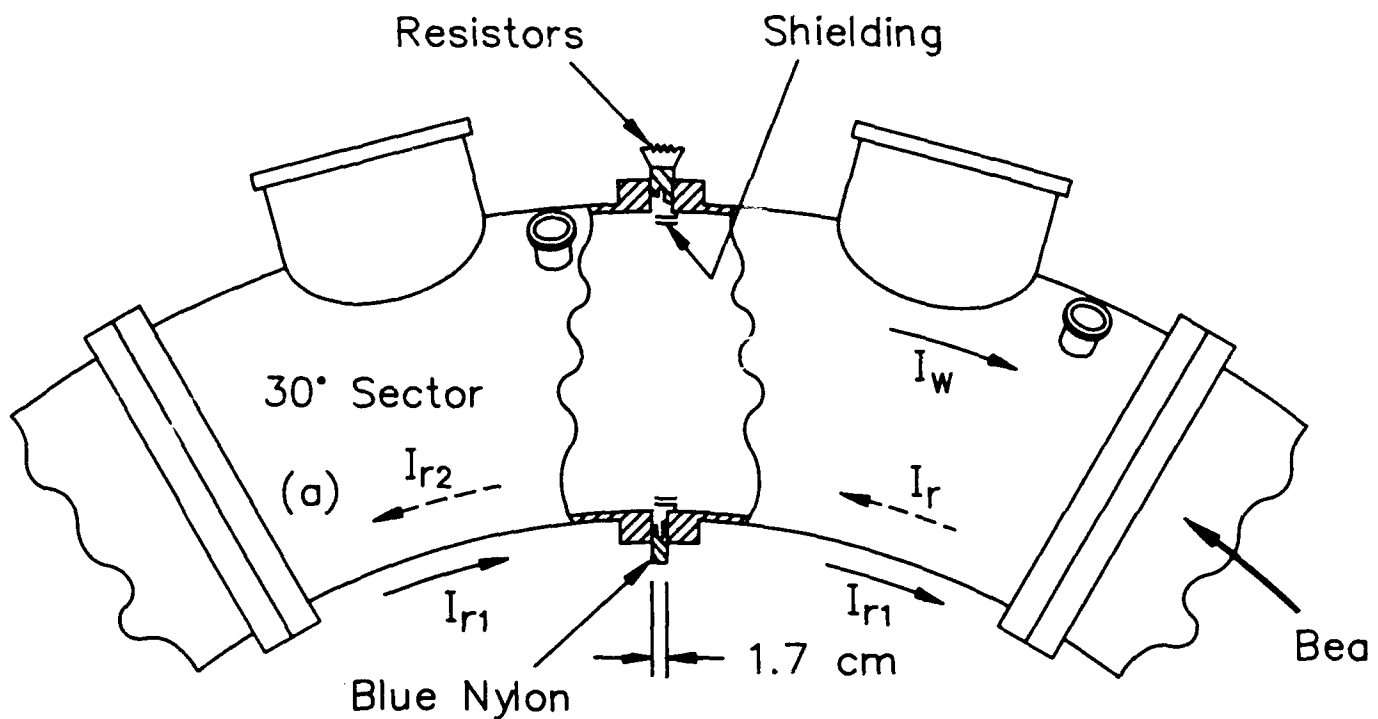


Fig. 4 — (a) Schematic of the vacuum chamber joint with the insulator in place.  
 (b) Current and gap voltage waveforms

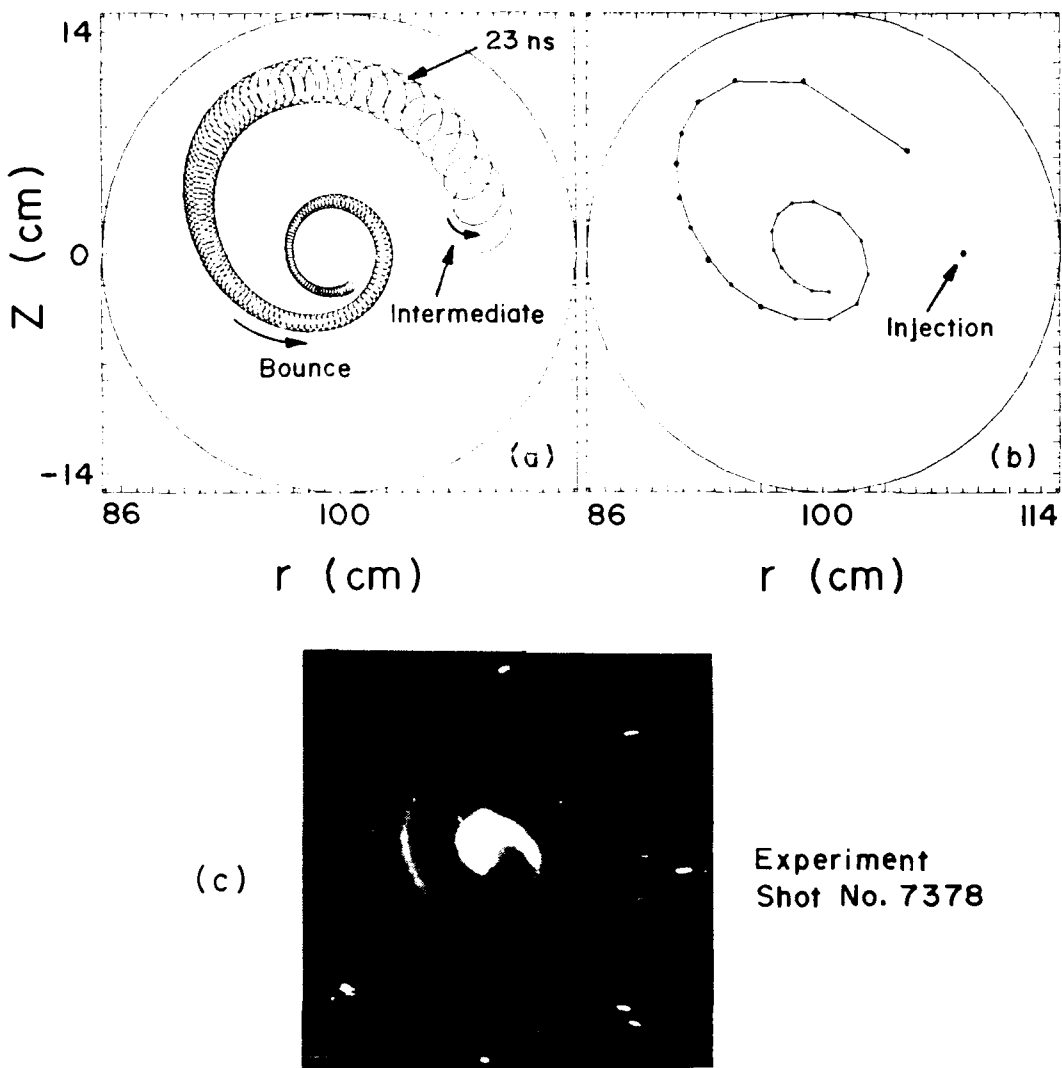


Fig. 5 — Beam centroid orbit from the numerical integration of the equations of motion, using the image fields from the resistive shell model (a and b). Results from the experiment (c).